**Journal of Computer Networks, Architecture and High Performance Computing**
Volume 6, Number 3, July 2024
https://doi.org/10.47709/cnapc.v6i3.4233

**Submitted** : 5 July 2024
**Accepted** : 9 July 2024
**Published** : 22 July 2024

# Geospatial Data Integration for the Flood Vulnerable Area Classification in Jratunseluna Watershed

**Humaid Assaidi[1)] , Muhammad Rokhis Khomarudin[2)] , Khairayu Badron[3)] , Ahmad Fadzil Ismail[4)] , Harry Ramza[5)*]**
[1),5)*]Department of Electrical Engineering, Faculty of Industrial Technology and Informatics, Universitas Muhammadiyah Prof. Dr. HAMKA, Indonesia
[2)]Research Center for Geomatic Science The National Agency of Research and Innovation, Republic of Indonesia
[3),4)]Satellite Communication and Technology Research Group, Department Electrical Engineering, Faculty of Engineering, International Islamic University of Malaysia, Malaysia
[1]assaidihumaid@gmail.com, [2]m.rokhis.khomarudin@brin.go.id, [3]khairayu@iium.edu.my,
[4]af_ismail@iium.edu.my, [5*]hramza@uhamka.ac.id

**ABSTRACT**
Flood is a threat that has significant impacts on communities and the environment. To improve the management of disaster risk, this research takes an integrated approach by utilizing geospatial data from various sources. The main objective of this research is to provide an integrated approach to determining flood-vulnerable area classes. This research focuses on the processing of various geospatial data such as DEM (Digital Elevation Model) imagery, Landsat 8 satellite imagery, Hydrological data based on SHuttle Elevation Derivatives at multiple Scales (HydroSHEDS) water flow accumulation imagery, and Climate Hazards Group InfraRed Precipitation with Station data (CHIRPS) rainfall imagery which are used as data sources to model the flood vulnerable area classification of The Jratunseluna watershed. Landsat 8 satellite imagery is used as a source for landuse land cover (LULC) classification, it is done to score each land category to the level of ability to absorb and drain excess water, the remaining data is used to score the earth elevation, accumulated water flow, and rainfall from the area. The weights and scores are used as the basis values to create a flood-vulnerable area classification model. The result of this research is a flood-vulnerable area classification map generated from a pre-made model.

**Keywords:** DEM; Landsat 8; HydroSHED; CHIRPS; LULC

## 1. INTRODUCTION

Flooding is a natural disaster that often causes huge losses to communities and the environment. It is a major highlight to identify potential flood areas in the disaster risk mitigation efforts. To develop effective risk management strategies, an in-depth understanding of an area's vulnerability to flooding is crucial. The significant impacts of a flood event include property loss, loss of life, and damage to vital infrastructure. Therefore, it is important to have an in-depth understanding of an area's vulnerability to flooding in order to design effective risk management strategies. The identification of factors that contribute to increase vulnerability to flooding is critical in the context of disaster risk management (Negese et all., 2022). Spatial and temporal variability of environmental components, such as land cover, topography, river flow, and rainfall patterns, are the focal points in the development of this flood vulnerability classification model.

The Jratunseluna river basin in Central Java Province, Indonesia, is frequently affected by flooding. However, there is a lack of a comprehensive model that integrates various geospatial data sources to accurately classify flood vulnerability in this area. This gap hampers effective risk management and mitigation efforts.

This study aims to develop a flood vulnerability classification model for the Jratunseluna watershed. By integrating geospatial data from multiple sources, such as Landsat 8 imagery for land cover analysis, DEM imagery for elevation modeling, HydroSHEDS imagery for river flow analysis, and CHIRPS rainfall imagery for rainfall patterns, the model seeks to enhance the understanding of flood risks in the area.

The study employs a geospatial data integration approach to classify flood vulnerability. This approach involves combining spatial and temporal variability of environmental components, such as land cover, topography,

* Corresponding Author

**Journal of Computer Networks, Architecture and High Performance Computing**
Volume 6, Number 3, July 2024
https://doi.org/10.47709/cnapc.v6i3.4233

**Submitted** : 5 July 2024
**Accepted** : 9 July 2024
**Published** : 22 July 2024

river flow, and rainfall patterns. The theoretical underpinning is based on the concept that integrating diverse environmental data sets can improve the accuracy and sustainability of flood risk mitigation efforts (Al-Areeq et al., 2023; Abdulrazzaq et al., 2018; Rahayu et al., 2023).

By utilizing geospatial data and integrating various environmental information, this research aims to contribute to a better understanding of flood risk. This, in turn, will enable more effective decision-making in the context of disaster management, ultimately enhancing the accuracy and sustainability of flood risk mitigation efforts.

## 2. LITERATURE REVIEW

Flood vulnerability assessment is a critical component in disaster risk management, particularly in regions prone to recurrent flooding. The integration of geospatial data has emerged as a pivotal method for evaluating flood vulnerability in various watersheds. Geographic Information System (GIS) techniques facilitate the merging of diverse datasets, such as rainfall, soil, topography, land use, drainage, and catchment flows, to effectively map flood-prone areas (Kunda et al., 2021). This integration enables a comprehensive examination of physical and socioeconomic factors, thereby identifying flood risk areas over different time periods (Bhuyan et al., 2023). The incorporation of remotely sensed data and other spatial information within GIS platforms has proven essential for creating thematic maps that aid in flood risk analysis and assessment. Research indicates that employing spatial multi-criteria evaluation methods within GIS environments is highly effective for estimating flood-vulnerable zones. These methods consider various physical factors, including rainfall intensity, slope, elevation, distance from rivers, land use, and soil type (Fadhil et al., 2020).

Despite significant advancements in GIS and remote sensing techniques, there remains a notable gap in the creation of a comprehensive model that integrates diverse geospatial data sources. Specifically, there is a lack of models that combine Digital Elevation Model (DEM) imagery, Landsat 8 satellite imagery, HydroSHEDS water flow accumulation imagery, and CHIRPS rainfall imagery to classify flood vulnerability in the Jratunseluna watershed. This gap highlights the need for further research to develop more integrated and accurate flood vulnerability models. The integration of geospatial techniques and GIS tools significantly enhances the assessment and analysis of flood vulnerability across various watersheds. By combining different datasets and employing advanced spatial analysis methods, researchers can effectively map flood-prone areas, assess vulnerability levels, and develop strategic mitigation measures. These efforts are vital for reducing the impact of floods in vulnerable regions and improving overall disaster management strategies. In summary, while current research has made substantial progress in the use of GIS and remote sensing for flood vulnerability assessment, there is a clear need for more comprehensive models that integrate multiple geospatial data sources. Addressing this gap will enable more accurate and sustainable flood risk mitigation efforts, particularly in the Jratunseluna watershed.

## 3. METHOD

In this research, 4 types of remote sensing data, namely DEM imagery (Xu et all., 2021)(Muhammed, 2020), Landsat 8 imagery, HydroSHEDS imagery, and CHIRPS imagery were used to create a classification model of the flood vulnerability in the area of interest. To create a flood vulnerability classification model, numerical values were extracted from the data as a reference. A new dataset derived from the 4 remote sensing data mentioned which contains a certain score and was obtained by a certain method which will be discussed later. By scoring, the degree to which the pixel value affects the occurrence of flooding can be measured. These scores can be used in subsequent steps to calculate a flood-vulnerable area classification model, where each type of data (DEM, land cover classification, accumulated water flow, rainfall) is weighted based on a predetermined score. Figure 1 is a flowchart that explains a summary of the steps taken in this study

* Corresponding Author

**Journal of Computer Networks, Architecture and High Performance Computing**
Volume 6, Number 3, July 2024
https://doi.org/10.47709/cnapc.v6i3.4233

**Submitted** : 5 July 2024
**Accepted** : 9 July 2024
**Published** : 22 July 2024

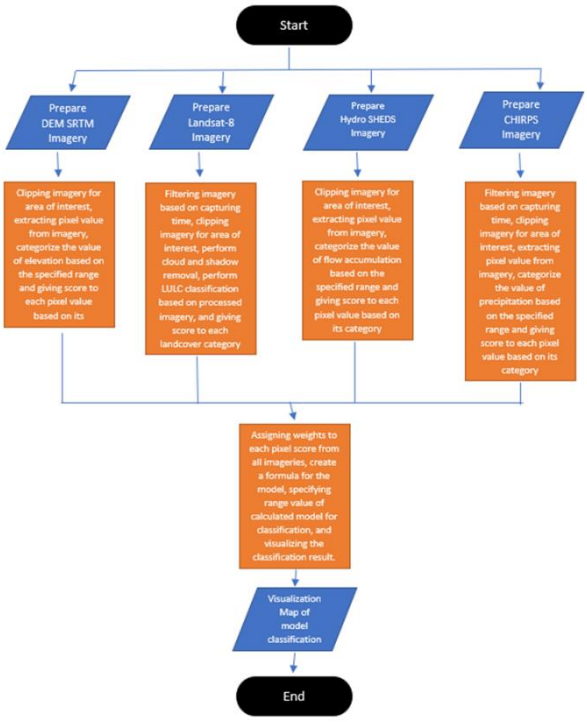


Fig.1 Flowchart of Research Steps.

In this research, the DEM imagery used is the Shuttle Radar Topography Mission (SRTM) image version 4 (Jarvis et all., 2008). This imagery contains data on the elevation of the earth's surface relative to the sea level. Extracting the numerical values were done by extracting pixel values in the DEM imagery of the area of interest. The pixel value was categorized based on the pixel value range and score was given to each range. The details of the scores for each range are described in Table 1.

Table 1
Scoring of DEM Imagery Pixel Values

| Condition | Score |
|---|---|
| Areas with pixel value equal to or less than 100 (elevation 100 m above sea level) | 10 |
| Areas with pixel value equal to or less than 500 but more than 100 | 5 |
| Areas with pixel values less than 500 | 1 |

To perform land-use land-cover (LULC) classification (Gn Vivekananda et all, 2021), Landsat 8 satellite imagery was used. Filtered imageries were capturedin 2021 for the area of interest. The cloud removal process had been carried out because clouds are noise in remote sensing imagery (Candra et all, 2017) (Shen et all, 2015). LULC classification in this study has 7 categories, namely vegetation, water bodies, built-up land, bush grass, open land, rice fields, and gardens. Before the LULC classification was conducted, Landsat 8 satellite imagery was first labelled based on each category. Furthermore, the classification was carried out using the random forest algorithm (Avci et all, 2023). After classification, each category is given a score or weight according to its potential contribution to flood vulnerability. The score for each land category depends on the ability of the particular land category to absorb water or drain excess water. The details of the scores given for each landcover category are described in Table 2.

* Corresponding Author

**Journal of Computer Networks, Architecture and High Performance Computing**
Volume 6, Number 3, July 2024
https://doi.org/10.47709/cnapc.v6i3.4233

**Submitted** : 5 July 2024
**Accepted** : 9 July 2024
**Published** : 22 July 2024

Table 2
Scoring of Landcover Category

| **Landcover** | **Score** |
|---|---|
| Water Body | 10 |
| Built-up Land | 10 |
| Bush Grass | 10 |
| Open Land | 10 |
| Rice Field | 5 |
| Garden | 5 |
| Vegetation | 1 |

In modeling the classification of flood-vulnerable areas, the accumulation of water flow on the land in the area of interest is also required to be known. This is the reason why the HydroSHEDS (Lehner et all, 2008) imagery was needed. The pixel values in the HydroSHEDS imagery were extracted so that the numerical values of the pixels can be used as a reference or data source for modeling. The pixel values from the HydroSHEDS image were then categorized based on their value range and scores were assigned for each range. Table 3 describes the scoring of each pixel value range.

Tabel 3
Scoring of Water-flow Accumulation

| **Condition** | **Score** |
|---|---|
| Areas with pixel values equal to or less than 150 | 1 |
| Areas with pixel values equal to or less than 500 but more than 150 | 5 |
| Areas with pixel values more than 500 | 10 |

Rainfall is also one of the factors that cause flooding (Narulita et all, 2018) (Auliyani et all, 2021). In this study, the use of rainfall data is considered as a reference in creating a flood-vulnerable land classification model. Due to the unavailability of 2021 data, CHIRPS (Funk et all, 2015) rainfall imagery that captured rainfall data throughout 2020 was used instead as the source of information. The data shows the rainfall level of the area of interest is represented by the pixel value. The mean and the standard deviation of the rainfall in a year within the area of interest were calculated to determine two thresholds. The mean and standard deviation of pixel values in rainfall imagery are used as mean and standard deviation of rainfall. The following is formula to get the mean and standard deviation of pixel value in imagery:

$$\text{Mean} = \frac{\sum_{i=1}^{h}\sum_{j=1}^{w} I_{ij}}{N} \quad (1)$$

$$\text{Standard Deviation} = \sqrt{\frac{\sum_{i=1}^{h}\sum_{j=1}^{w}\left(I_{ij} - \bar{I}\right)^2}{N}} \quad (2)$$

Description:
$I_{ij}$ = the intensity value of the pixel at row $i$ and column $j$ in the image.
$h$ = the height (number of rows) of the image.
$w$ = the width (number of columns) of the image.
$N$ = the total number of pixels in the image, which is equal to $h \times w$.
$\bar{I}$ = the mean pixel value of the image.

* Corresponding Author

**Journal of Computer Networks, Architecture and High Performance Computing**
Volume 6, Number 3, July 2024
https://doi.org/10.47709/cnapc.v6i3.4233

**Submitted** : 5 July 2024
**Accepted** : 9 July 2024
**Published** : 22 July 2024

The first threshold, labeled as 'Threshold 1' was obtained from the mean value of the rainfall, minus the standard deviation. Meanwhile, the second threshold, identified as 'Threshold 2' was obtained from the mean of the rainfall, plus the standard deviation. After obtaining threshold values 1 and 2, the pixel values of the rainfall image were scored. Table 4 shows the details of the scores.

Table 4
Scoring of Rainfall

| Condition | Score |
|---|---|
| The rainfall value at a pixel is less than or equal to the threshold 1 | 1 |
| The rainfall value at a pixel is more than threshold 1 but less than or equal to threshold 2 | 5 |
| The rainfall value at a pixel is more than the threshold 2 | 10 |

The flood vulnerable area classification model was calculated by combining scores from the above four factors: elevation (DEM score), landcover (landcover score), water-flow accumulation (water-flow accumulation score), and rainfall (rainfall score). Each score is given a certain weight according to its contribution. The weights that had been proposed to create the model are as follows:

$$Model = (elevation\ score\ x\ 0.2) + (landcover\ score\ x\ 0.25) + (waterflow\ accumulation\ score\ X\ 0.25) + (rainfall\ score\ x\ 0.3) \quad (3)$$

The values of 0.2, 0.25, 0.25, and 0.3 in the formula above are the weights given to each factor that affects the occurrence of the flood. The values of weight that mentioned earlier are discovered from the tuning experiment in google earth engine. These weights are the most optimum values in this particular study area. This model can be used based on expert judgment (Rokhis Research Group, 2024) conducted through group discussions and the delphi technique, which involves collecting opinions and feedback from a panel of anonymously selected experts through several rounds of questionnaires.

This weight indicates the value of a factor that affects the occurrence of floods. It can be strengthened or weakened because the factors that most affect the occurrence of floods in an area are always different depending on the conditions of the area in terms of topography, land use, rainfall, water-flow accumulation, and elevation. (Mahmud et all, 2018). In the case of high rainfall in areas with high elevation, the high rainfall does not affect the vulnerability of the area to flooding.

After calculating the model, statistical calculations, such as mean and standard deviation were performed on the area of interest. These we re carried out to understand the spatial variation of the flood vulnerable area classification model. The threshold for flood vulnerable area classification was determined based on the mean and standard deviation values of the model just like the threshold calculation for the rainfall. Using these thresholds, the model was categorized, and each category was scored, and each pixel was assigned a flood-vulnerable area class according to its threshold. The result is a map of flood-vulnerable areas that divides the area of interest into three classes: Low, Medium, and High. This map helps in understanding the extent to which an area can be vulnerable to potential flooding, providing important insights for flood risk planning and mitigation. Visualizing the classification results on a map facilitates spatial interpretation to support decision-making related to flood risk management.

## 4. RESULT

Figure 2 is the visualization map of DEM values from SRTM images for the areas of interest which had been categorized based on the value ranges explained in the methodology.

* Corresponding Author

**Journal of Computer Networks, Architecture and High Performance Computing**
Volume 6, Number 3, July 2024
https://doi.org/10.47709/cnapc.v6i3.4233

**Submitted** : 5 July 2024
**Accepted** : 9 July 2024
**Published** : 22 July 2024

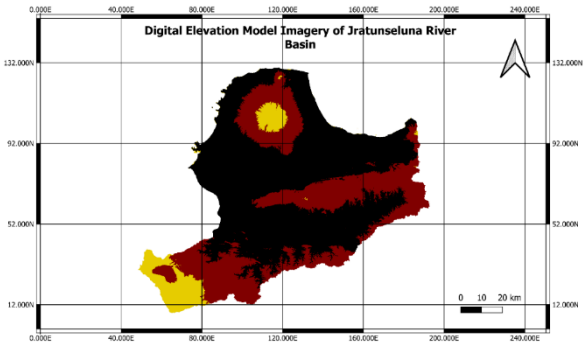


Fig. 2 Map of Elevation Classification Based on DEM Imagery.

To understand the distribution of the earth's elevation on the map, the meaning of the colors on the map needs to be known. Table 5 explains the details of the meaning of the colors on the map.

Table 5: Meaning of Color in Elevation Classification Map.

| Color | Meaning |
|---|---|
| Black | Areas with elevation value equal to or less than 100m above sea level |
| Maroon | Areas with elevation value equal to or less than 500m but more than 100m above sea level |
| Yellow | Areas with elevation value more than 500m above sea level |

From the elevation visualization map above, it is known that more than 50% of the area of interest is lowland below 100 meters above sea level. To carry out LULC classification, the Landsat 8 satellite imagery was used as the reference as discussed in the methodology. Figure 3 below is a Landsat 8 satellite imagery visualized in RGB or true color mode by selecting the red (b4), green (b3), and blue (b2) bands. Not forgetting that the image has also gone through the cloud filtering stage. That Clouds typically prevents the satellite from capturing the earth's surface picture.

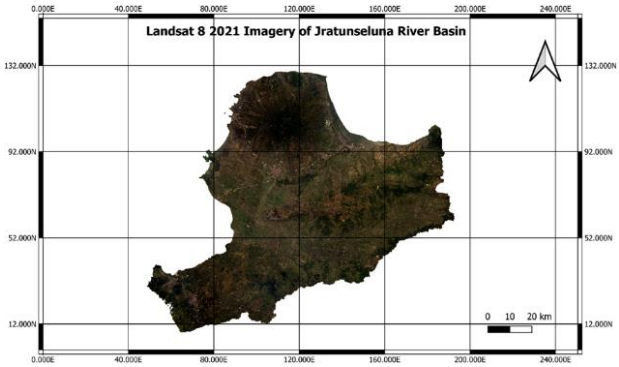


Fig. 3 Landsat 8 2021 Imagery of Area Interest.

Figure 4 below is a visualization map of the LULC classification results in the area of interest.

* Corresponding Author

**Journal of Computer Networks, Architecture and High Performance Computing**
Volume 6, Number 3, July 2024
https://doi.org/10.47709/cnapc.v6i3.4233

**Submitted** : 5 July 2024
**Accepted** : 9 July 2024
**Published** : 22 July 2024

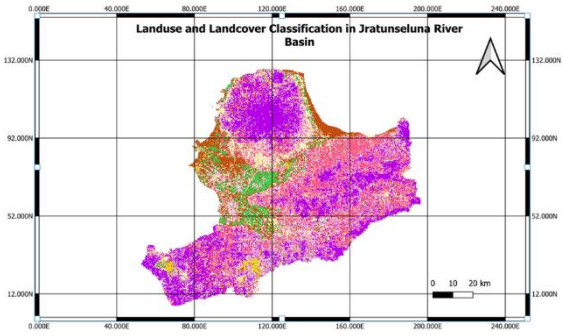


Fig. 4 Map of Landuse and Landcover Category in Area of Interest.

The meaning of the colors on the LULC classification map is explained in Table 6.

Table 6
Meaning of Color in Landuse and Landcover Classification Map.

| Color | Landcover Category |
|---|---|
| Yellow | Water Body |
| Cream | Built-up Land |
| Lavender | Bush Grass |
| Pink | Open Land |
| Brown | Rice Field |
| Green | Garden |
| Purple | Vegetation |

Based on the LULC classification, the largest area of interest is vegetation, followed by open land and gardens. To understand the water flow accumulation pattern, Figure 5 was generated. It is the visualization map of the water flow accumulation values from the HydroSHEDS imagery which it can help an easier understanding of the water flow accumulation pattern in the area of interest.

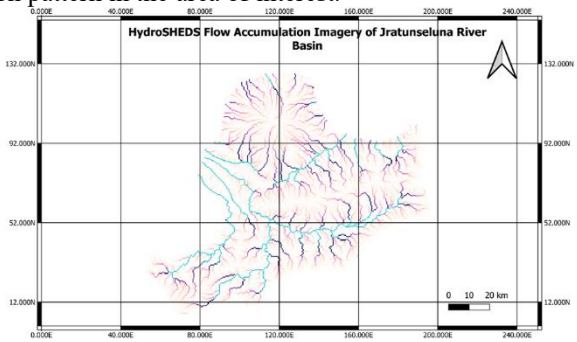


Fig. 5 Map of Flow Accumulation in Area of Interest.

The cyan-blue area is the area with the highest water accumulation, followed by purple, brown, and white. The CHIRPS imagery was also processed to understand the level of rainfall in the area of interest for the year. Figure 6 is the map that depicts visualization and categorizes the rainfall value.

* Corresponding Author

**Journal of Computer Networks, Architecture and High Performance Computing**
Volume 6, Number 3, July 2024
https://doi.org/10.47709/cnapc.v6i3.4233

**Submitted** : 5 July 2024
**Accepted** : 9 July 2024
**Published** : 22 July 2024

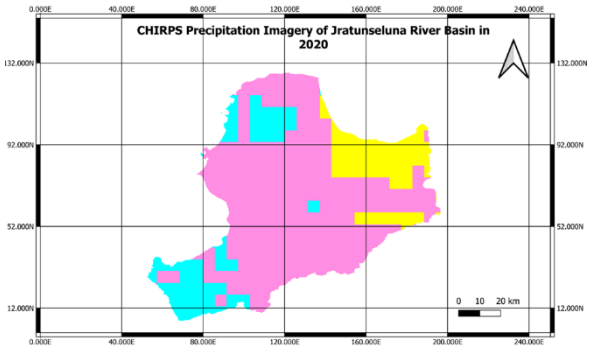


Fig. 6 Map of Rainfall Level of Area of Interest in 2020.

Understand the level of rainfall level in areas of interest, Table 7 describes the meaning of each color in the map.

Table 7
Meaning of Color in Precipitation (Rainfall) Classification Map.

| Color | Meaning |
|---|---|
| Yellow | Areas with precipitation value equal to or less than 2350.300 mm/year |
| Pink | Areas with precipitation value equal to or less than 2931.772 mm/year but more than 2350.300 mm/year |
| Cyan | Areas with precipitation value more than 2350.300 mm/year |

After calculating the average rainfall and its standard deviation for the year in the area of interest, the following values were obtained. The average rainfall in the area of interest is 2641,036 mm/year and the standard deviation is 290,736 mm/year. From the two mentioned values , the threshold 1 value is 2350,300 mm/year (threshold 1 is obtained from subtracting the average from the standard deviation) and the threshold 2 value is 2931,772 mm/year (threshold 2 is obtained from adding the average to the standard deviation). As discussed in the methodology, threshold values 1 and 2 are then used as a reference in calculating the rainfall score.

After the dataset for creating the flood vulnerable area classification model was successfully created, the the average and standard deviation of the model were determined. The mean and standard deviation that were obtained from the model are 5,043 and 1,322. Flood vulnerable area classification was carried out by categorizing values from the model that are below threshold 1. These are the areas with a low level of flood vulnerability, while values between threshold 1 and 2 are areas with a medium flood vulnerability level. For those with values above threshold 2 are basically areas with a high flood vulnerability level. After the calculations were carried out, the flood hazard classification category model can be visualized by map shown in Figure 7. And the meaning of colors in the map are described in Table 8.

* Corresponding Author

**Journal of Computer Networks, Architecture and High Performance Computing**
Volume 6, Number 3, July 2024
https://doi.org/10.47709/cnapc.v6i3.4233

**Submitted** : 5 July 2024
**Accepted** : 9 July 2024
**Published** : 22 July 2024

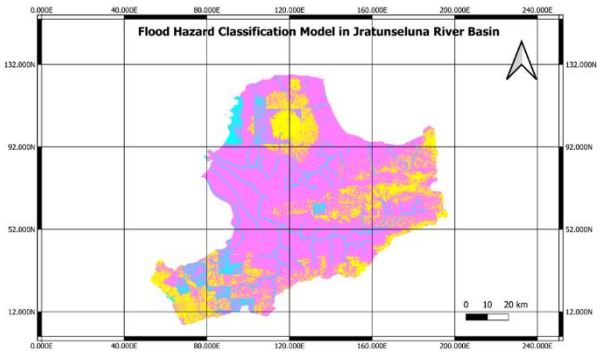

Fig. 7 Map of Flood Vulnerable Area Classification.

Table 8
Meaning of Color in Map of Flood Vulnerable Area Classification.

| Color | Meaning |
|---|---|
| Yellow | Areas with low flood vulnerability levels |
| Pink | Areas with medium flood vulnerability levels |
| Cyan | Areas with high flood vulnerability levels |

## 5. CONCLUSION

The research findings presented in this study reveal significant insights into the flood vulnerability of the Jratunseluna watershed. Elevation data analysis indicates that over 50% of the watershed comprises lowland areas, situated below 100 meters above sea level. This elevation classification, derived from Shuttle Radar Topography Mission (SRTM) images, is crucial for understanding the region's susceptibility to flooding. Additionally, the Land Use and Land Cover (LULC) classification, utilizing Landsat 8 satellite imagery, identified seven distinct categories: vegetation, water bodies, built-up land, bush grass, open land, rice fields, and gardens. Vegetation emerged as the dominant land cover category, followed by open land and gardens. This classification aids in comprehending the area's water absorption and drainage capacities. The study also incorporated water flow accumulation data from HydroSHEDS imagery, highlighting areas with the highest water accumulation in cyan-blue, followed by purple, brown, and white areas. This mapping provides valuable insights into potential flood-prone zones. Furthermore, the analysis of CHIRPS rainfall imagery from 2020 revealed an average annual rainfall of 2641.036 mm, with a standard deviation of 290.736 mm. This rainfall data was categorized into three thresholds to score and map flood vulnerability based on rainfall intensity. By integrating scores from DEM, LULC, water flow accumulation, and rainfall data, the study developed a comprehensive flood vulnerability classification model. The model assigned specific weights to each factor, resulting in a map categorizing flood vulnerability into low, medium, and high levels. The majority of the Jratunseluna watershed was found to fall under medium to high flood vulnerability categories, indicating a significant risk of flooding. In conclusion, the study successfully created a flood vulnerability classification model for the Jratunseluna watershed by integrating various geospatial data sources. The findings underscore the region's topographic characteristics, land cover distribution, water flow patterns, and rainfall levels, all contributing to the flood vulnerability assessment. The generated flood vulnerability map provides critical insights for disaster risk management and mitigation efforts in the region, assisting authorities in prioritizing areas for intervention and developing effective flood risk management strategies.

## 6. ACKNOWLEDGEMENTS

This research was conducted at the Research Center for Geomatics, The Agency of National Research and Innovation (BRIN), District Cibinong, Municipality of Bogor, Republic of Indonesia. All research staff provided invaluable inspiration and guidance throughout the development of the classification model, offering insights into
* Corresponding Author

**Journal of Computer Networks, Architecture and High Performance Computing**
Volume 6, Number 3, July 2024
https://doi.org/10.47709/cnapc.v6i3.4233

**Submitted** : 5 July 2024
**Accepted** : 9 July 2024
**Published** : 22 July 2024

methodologies and potential steps to undertake. The research activity is one of the government programs on Independent Learning of Independent Campus Program, Batch 2023-2024, between UHAMKA and the Research Center for Geomatics, BRIN.

## 7. REFERENCES

Jarvis, A., Reuter, H. I., Nelson, A., & Guevara, E. (2008). Hole-filled SRTM for the globe Version 4. Available from the CGIAR-CSI SRTM 90m Database: https://srtm.csi.cgiar.org

Lehner, B., Verdin, K., & Jarvis, A. (2008). New global hydrography derived from spaceborne elevation data. Eos, Transactions, AGU, 89(10), 93-94.

Funk, C., Peterson, P., Landsfeld, M., Pedreros, D., Verdin, J., Shukla, S., ... & Michaelsen, J. (2015). The climate hazards infrared precipitation with stations-a new environmental record for monitoring extremes. *Scientific Data, 2*, 150066. doi: https://doi.org/10.1038/sdata.2015.66

Avcı, C., Budak, M., Yağmur, N., & Balçık, F. (2023). Comparison between random forest and support vector machine algorithms for LULC classification. *International Journal of Engineering and Geosciences, 8*(1), 1-10. doi: https://doi.org/10.26833/ijeg.987605

Gn Vivekananda, R Swathi, & AVLN Sujith. (2021). Multi-temporal image analysis for LULC classification and change detection. *European Journal of Remote Sensing, 54*(sup2), 189-199. doi: https://doi.org/10.1080/22797254.2020.1771215

Candra, D. S., Phinn, S., & Scarth, P. (2017). Cloud and cloud shadow removal of Landsat 8 images using Multitemporal Cloud Removal method. *2017 6th International Conference on Agro-Geoinformatics*, 1-5. doi: https://doi.org/10.1109/Agro-Geoinformatics.2017.8047007

Shen, Y., Wang, Y., Lv, H., & Li, H. (2015). Removal of thin clouds using Cirrus and QA bands of Landsat-8. *Photogrammetric Engineering & Remote Sensing, 81*(9), 721-731. doi: https://doi.org/10.14358/PERS.81.9.721

Al-Areeq, A. M., Sharif, H. O., Abba, S. I., Chowdhury, S., Al-Suwaiyan, M., Benaafi, M., ... & Aljundi, I. H. (2023). Digital elevation model for flood hazards analysis in complex terrain: Case study from Jeddah, Saudi Arabia. *International Journal of Applied Earth Observation and Geoinformation, 119*, 103330. doi: https://doi.org/10.1016/j.jag.2023.103330

Bhuyan, M., Deka, N., & Saikia, A. (2023). Micro-spatial flood risk assessment in nagaon district, assam (india) using gis-based multi-criteria decision analysis (mcda) and analytical hierarchy process (ahp). Risk Analysis, 44(4), 817-832. https://doi.org/10.1111/risa.14191

Fadhil, M., Ristya, Y., Oktaviani, N., & Kusratmoko, E. (2020). Flood vulnerability mapping using the spatial multi-criteria evaluation (smce) method in the minraleng watershed, maros regency, south sulawesi. E3s Web of Conferences, 153, 01004. https://doi.org/10.1051/e3sconf/202015301004

Karmakar, S., Simonović, S., Peck, A., & Black, J. (2010). An information system for risk-vulnerability assessment to flood. Journal of Geographic Information System, 02(03), 129-146. https://doi.org/10.4236/jgis.2010.23020

Kunda, J., Jajere, A., Otabe, E., Muhammed, C., Bibi, U., & Maina-Bukar, Y. (2021). Empirical model valuation of urban agriculture vulnerability to flooding in makurdi, benue state, nigeria. Environment and Pollution, 10(2), 20. https://doi.org/10.5539/ep.v10n2p20

Meraj, G., Romshoo, S., Yousuf, A., Altaf, S., & Altaf, F. (2015). Assessing the influence of watershed characteristics on the flood vulnerability of jhelum basin in kashmir himalaya: reply to comment by shah 2015. Natural Hazards, 78(1), 1-5. https://doi.org/10.1007/s11069-015-1861-0

Nkeki, F., Henah, P., & Ojeh, V. (2013). Geospatial techniques for the assessment and analysis of flood risk along the niger-benue basin in nigeria. Journal of Geographic Information System, 05(02), 123-135. https://doi.org/10.4236/jgis.2013.52013

Prasad, B., Rao, P., Ramamohanarao, P., & Sarathkumar, S. (2022). Flood hazard vulnerability assessment by using geo spatial techniques: krishna and guntur districts, andhra pradesh. Current World Environment, 17(2), 498-506. https://doi.org/10.12944/cwe.17.2.20

Xu, K., Fang, J., Fang, Y., et al. (2021). The Importance of Digital Elevation Model Selection in Flood Simulation and a Proposed Method to Reduce DEM Errors: A Case Study in Shanghai. *International Journal of Disaster Risk Science, 12*, 890–902. doi: https://doi.org/10.1007/s13753-021-00377-z

* Corresponding Author

**Journal of Computer Networks, Architecture and High Performance Computing**
Volume 6, Number 3, July 2024
https://doi.org/10.47709/cnapc.v6i3.4233

**Submitted** : 5 July 2024
**Accepted** : 9 July 2024
**Published** : 22 July 2024

Muhammed, I. (2020). Flood mapping and simulation using Sentinel 2 and SRTM data. FUTY Journal of the Environment, 14(1).

Abdulrazzaq, Z. T., Aziz, N. A., & Mohammed, A. A. (2018). Flood modelling using satellite-based precipitation estimates and digital elevation model in eastern Iraq. *International Journal of Advanced Geosciences, 6*(1), 72-77. doi: 10.14419/ijag.v6i1.8946

Rahayu, R., Mathias, S. A., Reaney, S., et al. (2023). Impact of land cover, rainfall and topography on flood risk in West Java. *Natural Hazards, 116*, 1735–1758. doi: https://doi.org/10.1007/s11069-022-05737-6

Negese, A., Worku, D., Shitaye, A., et al. (2022). Potential flood-prone area identification and mapping using GIS-based multi-criteria decision-making and analytical hierarchy process in Dega Damot district, northwestern Ethiopia. *Applied Water Science, 12*, 255. doi: https://doi.org/10.1007/s13201-022-01772-7

Narulita, I., & Ningrum, W. (2018, February). Extreme flood event analysis in Indonesia based on rainfall intensity and recharge capacity. *IOP Conference Series: Earth and Environmental Science, 118*(1), 012045. doi: https://dx.doi.org/10.1088/1755-1315/118/1/012045

Auliyani, D., & Wahyuningrum, N. (2021, October). Rainfall variability based on the Climate Hazards Group InfraRed Precipitation with Station Data (CHIRPS) in Lesti watershed, Java Island, Indonesia. *IOP Conference Series: Earth and Environmental Science, 874*(1), 012003. doi: https://dx.doi.org/10.1088/1755-1315/874/1/012003

Mahmud, A., Kusumandari, A., Sudarmadji, S., & Supriyatno, N. (2018). A Study of Flood Causal Priority in Arui Watershed, Manokwari Regency, Indonesia. Jurnal Manajemen Hutan Tropika, 24(2), 81-94. DOI: 10.7226/jtfm.24

* Corresponding Author